Fractal quantum transport in systems with mixed phase space

Anas Ahmad Rana

May 20, 2008

Contents

Chapter 1

Introduction

Chapter 2

Background

2.1 Classical kicked rotor

2.1.1 Derivation of the Standard Map

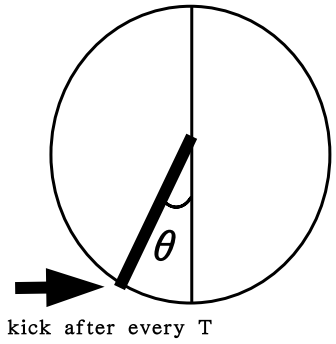

Figure 2.1: The kicked rotor with Periodic Kicks

The Hamiltonian of the kicked rotor reads

$$H(L,\theta,t) = \frac{L^2}{2I} + k\ \cos(\theta)\sum_n \delta(t-nT) \tag{2.1}$$

where L is the angular momentum, I the momentum of inertia, S is the kick-strength, $\delta(t-nT)$ is the Dirac delta function, T is the period of kicks and θ is the angular position of the rotor. The first term of the Hamiltonian is the kinetic energy term for a rotor. The second term is the potential from applying δ-kicks in a period of T. The corresponding Hamiltonian equations of motion for (1) are given by

$$\begin{aligned} \dot{L} &= -\frac{\partial H(L,\theta,t)}{\partial \theta} = k\ \sin(\theta)\sum_n \delta(t-nT) \\ \dot{\theta} &= \frac{\partial H(L,\theta,t)}{\partial L} = \frac{L}{I}. \end{aligned} \tag{2.2}$$

The angular momentum changes discontinuously across kicks whereas θ is continuous. Between kicks there are periods of free motion. We denote L_j and θ_j as the values of the rotor immediately before kick j and $L_j^{'}$ and $\theta_j^{'}$ as the values of the rotor immediately after kick j. Integrating (2) over the infinitesimal time-interval of the kick we obtain

$$L_j^{'} - L_j = k\ \sin(\theta_j), \tag{2.3}$$

additionally we have

$$\theta_j^{'} = \theta_j. \tag{2.4}$$

During the periods of free motion L is conserved (L_{j+1} just before kick $j+1$ L_j) and θ varies according to equation (2), therefore we get

$$\begin{aligned} L_{n+1} &= L_n + k\ \sin(\theta_n) \\ \theta_{n+1} &= \theta_n + \frac{T\,L_{n+1}}{I} \end{aligned} \tag{2.5}$$

We set $l_j = L_j\,T/I$ which means measuring the angular momentum in units of I/T, we also set $S = k\,T/I$, to obtain the dimensionless mapping equations

$$\begin{aligned} l_{n+1} &= l_n + S\ \sin(\theta_n) \\ \theta_{n+1} &= \theta_n + l_{n+1} \end{aligned} \tag{2.6}$$

From the equations, we can see, that the phase space has a symmetry of 2π in l as well as in θ. Therefore we only plot the unit cell of modulo 2π both in l and θ. Given a set of initial conditions in phase space it is possible to determine if the trajectory is simple or complex. To see more structure in phase space we take a set of initial conditions. The only parameter in this case is S the kick-strength. When increasing S, we expect the phase space to become more chaotic. To observe this we draw phase spaces with different values of S.

We can see here, that increasing S leads to a more chaotic phase space, as expected. Starting with $S = 2$ we see a phase space with a large regular structure, that has its fixed point of order one at $l = 0$, $\theta = \pi$, this regular region is enclosed in a seperatrix. There is also a fixed point of second order, which is split into because of the boundaries chosen for the phase space, at $l = \pi$ and $l = -\pi$ and some higher order fixed points just outside the seperatrix in the centre of the phase space. At higher S the regular structures in phase space decrease in size. Already at $S = 4$, the fixed points at $l = \pm\pi$ are not visible on the chosen scale. From $S = 4$ to $S = 5$ we observe how the regular elliptical island in the middle of the unit cell breaks up. At $S = 7$ there are no more regular structures visible, and the whole phase space is globally chaotic on the usual scale. There still are some fixed points, but they are very small. The phase space of the kicked rotor is only globally chaotic on all scales for $S \to \infty$.

The first chaotic regions in phase space appear for $S \approx 0.9$ as the value quoted in literature. The value quoted for the onset of chaos on the usual scale is $S \approx 5$. On the scale used here there were still some regular structures at $S = 6$, but there size was already quite small.

The lines drawn in phase space plots for $S = 4, 5, 7$ are in the chaotic Region of phase space are important for the discussion of the energy and decay in the following sections. These lines specify initial conditions for trajectories in the chaotic region.

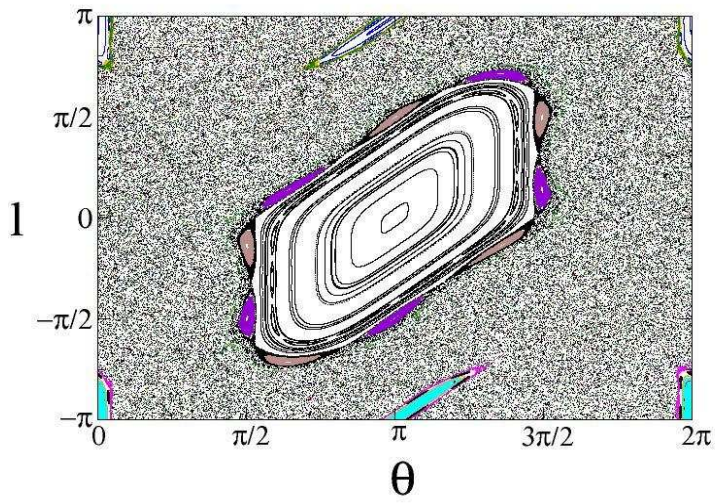

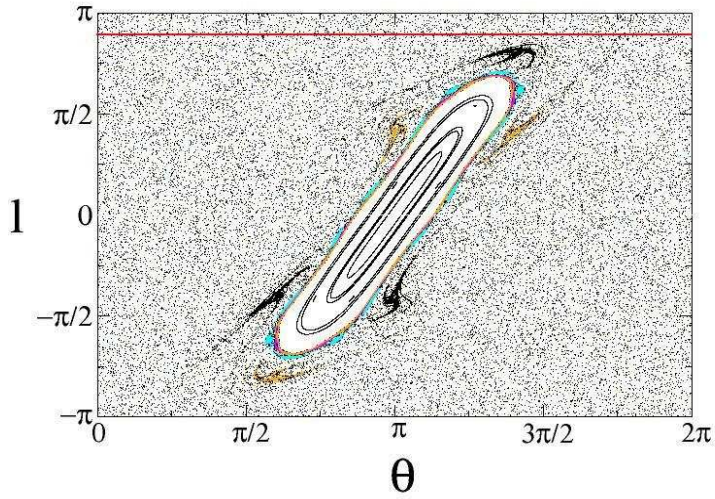

For $S = 2$ it is not in fact possible to find such a line, hence a square grid with initial points will be used. Since in the classical phase space these trajectories cannot cross over into the regular regions.

2.1.2 Energy

To get the energy for the kicked rotor as a function of kicks, we need to calculate $E = l^2/2$ from (2.6);

$$E_n = \frac{l_n^2}{2} = E_{n-1} + \frac{S^2 \, \sin^2(\theta_n)}{2} + \, S \, l_{n-1} \, \sin(\theta_n). \tag{2.7}$$

Applying this equation recursively for E on right hand side of the equation we

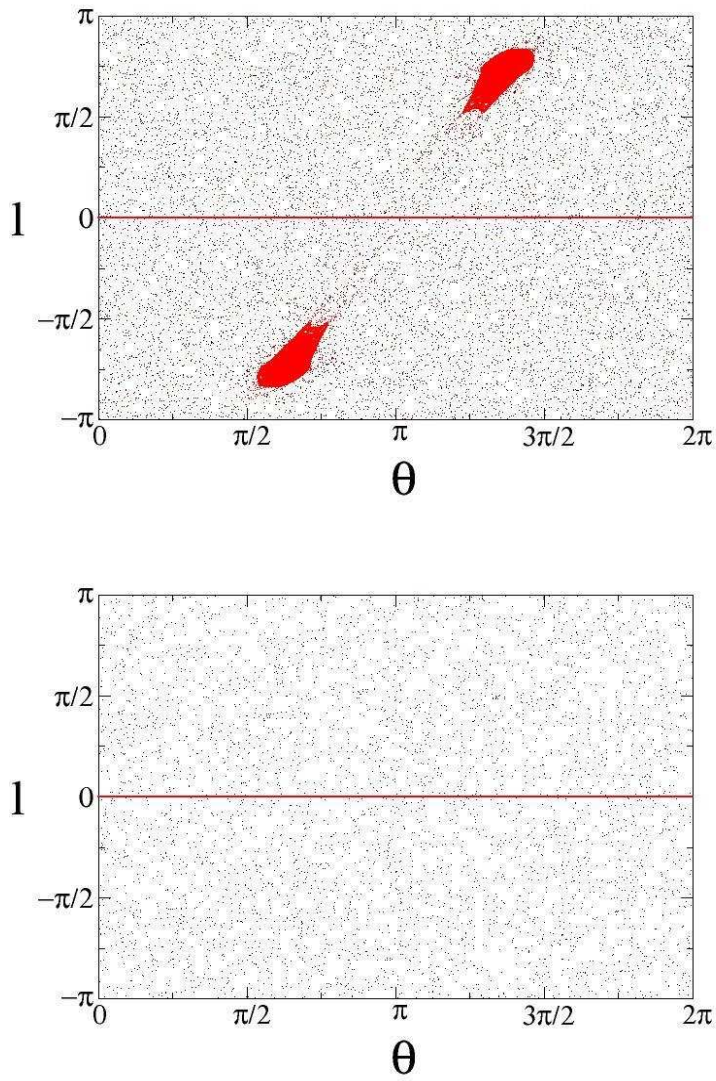

Figure 2.2: phase space plots for different values of S.
top left: S=2, top right: S=4, bottom left: S=5, bottom right: S=7

get

$$E_n = E_0 + \sum_{i=0}^{n-1} \left(\frac{S^2 \sin^2(\theta_i)}{2} + a_i \sin(\theta_i) \right) \tag{2.8}$$

now if we take an average over the number of kicks in the chaotic region, $\sin^2(\theta_i) = 1/2$ and $\sin(\theta) = 0$. Therefore we get the approximation

$$E_n \approx E_0 + \frac{S^2 n}{4}. \tag{2.9}$$

If we now plot E_n as a function of n, the expected straight line has the gradient

$$D = S^2/4 \tag{2.10}$$

it is necessary to specify initial conditions which are in the chaotic regime, because the above equation only applies to trajectories which are unbound, i.e. they evolve freely. If the trajectories are started in the regular regions of phase space, they stay inside the seperatrix and the Energy cannot grow freely. The best way to come close to this in a phase space with bound regular structures separated from the chaotic part, is to choose the initial condition in the chaotic part, which minimises the probability of trapped trajectories. The reason is, that even when starting in the chaotic regions some trajectories come close to a seperatrix and get trapped around this structure.

The dashed line represents initial values in a $900 * 900$ grid, the solid line initial values in a $30 * 30$ grid and the dotted line the time average. The solid straight line is the expected Energy growth from (2.9). The grids for the initial values are chosen in the chaotic region of phase space.

S	2	2.2	3	4	5	6	7
line (ensemble ave)		0.25	2.10	2.89	6.18	13.62	36.98
line (time ave)		0.13	0.99	1.41	3.05	7.10	20.25
square 900*900 (ens)	0.19	0.29	2.15	3.09	6.31	14.34	37.50
square 300*300 (ens)	0.31	0.29	2.23	2.91	5.90	15.49	39.24
predicted	1	1.21	2.25	4	6.25	9	12.25

Table 2.1: gradients of different ensembles and kick strengths

For $S = 2$ we see a straight line for the energy against time as expected, but the gradient of the line is not as predicted by equation (2.10). The main reason for this discrepancy is, that the trajectories in the phase space get trapped around the regular regions, which results in an energy change which is not the expected linear growth according to equation (2.9).

For $S = 5$ where most of the phase space is chaotic we do not see the skewing of the graph due to trapped trajectories as expected. The gradient of the curve with an average over the ensemble of initial conditions is 6.31 (for an ensemble of 900*900 square grid, compare with Table 1), which is close to the expected value of $D = 6.25$.

Looking at the case with $S = 7$, we see that the proximity for the expected value and the actual gradient at $S = 5$ are only by chance. $S = 7$ yields a completely chaotic phase space, but $D \neq S^2/4$. According to Rechester and White (1980) equation (2.10) is an approximation to the actual value of D, which in fact oscillates around the mean value $\bar{D}$ (equation (2.10)), which is a good approximation for $S \gg 1$, because the oscillations have died down. There are also effects due to "accelerator modes" (Chirikov (1979)) in the phase space, thought these effect only play a role for values of S which have regular structures in the phase space.

2.1.3 Decay

Looking at motions in the chaotic regime, we define a trajectory as *decayed*, after it enters a defined strip bound in phase space by a l_1 and l_2. Once a trajectory has

"decayed" we discard it, because it could jump out of the strip and than back in to "decay" again, which would distort our findings. Now we plot the number of decays against n. If we define this decay in the whole cylinder, for S with large regular structures some of the trajectories get trapped around accelerator modes and jump with steps $\approx 2\pi$, changing the graph of decayed values. Since the cylinder is also periodic in 2π for l, it is possible to take value of l modulo 2π. All the trajectories need to be started in the chaotic regime, because otherwise we could not observe any decays, since the trajectories would be trapped in the regular regions. We plot decay rates against n for different S. The values of S are chosen to have different amounts of regular structures in the phase space.

The figures all have initial points in a $900 * 900$ grid in the chaotic part of phase space. The decay-strip was chosen with $l = 2.6 - 2.8$. The decay rate for $S = 2$ follows an exponential decay for the first 100 kicks, after that the decay rate gradually approaches a power law. As it can be observed from the plots, for increasing S the exponential curve becomes a better approximation for the decay rate. For large n, all plots have steps, this is due to the fact that the number of decays is very small and insufficient for the statistic.
If we plot the phase space for the decay, we see regular structures emerging (see Fig. 2.5). These structures resembles a strange repeller in phase space. A repeller is a structure that repels all trajectories that come close to it. The large white space, that can be observed for the phase space of $S = 4$ around $\theta = \pi$ and $l = \pm\pi/2$ comes from the regular structure, that is bound by a separatrix of the phase space as can be seen in Fig (2.2), though in this case l goes from 0 to 2π.

2.2 Quantum kicked rotor

2.2.1 Derivation of the Quantum Map

The Quantum version of the δ-kicked rotor can also be realised experimentally as mentioned in 1. The quantum mechanical Hamiltonian for this system can be derived from (2.1), by replacing the classical angular momentum L by the quantum mechanical angular momentum operator $\hat{L} = -i\,\hbar\,\partial/\partial\theta$. Therefore the Hamiltonian operator reads

$$\hat{H} = \frac{\hat{L}^2}{2\,I} + K\cos(\hat{\theta})\sum_n \delta(t - nT). \tag{2.11}$$

Like in the classical case, the quantum mechanical Hamiltonian is also periodic, but the wave function is not. This can be remedied by applying Bloch's Theorem, which reduces it to a periodic problem with an additional parameter for the system. Bloch's theorem states, that for a system with periodic potential the wave function can be split into two components. One is the phase factor and the other is the periodic part of the wave function

$$\psi(\theta) = e^{i\beta\theta}\,u(\theta);\; u(a) = u(-a) \tag{2.12}$$

where β is the quasimomentum, a conserved quantity hence also a parameter of the system. The quasimomentum is also the decimal part of the momentum $L = n + \beta$, where $n\,\epsilon\,\mathbb{N}$ and $\beta\,\epsilon[0, 1[$. Since β is constant, it is possible to write the momentum

operator as $\hat{L} = \hat{n} + \beta$, resulting in the Hamiltonian

$$\hat{H} = \frac{(\hat{n} + \beta)^2}{2\,I} + K\cos(\hat{\theta}) \sum_n \delta(t - nT) \tag{2.13}$$

To get an expression for the evolution of the quantum kicked rotor as a function of time, the quantum mapping operator needs to be evaluated. For this system it is the Unitary time evolution operator, which can be derived from the Schrödinger equation

$$i\,\hbar\,\frac{\partial}{\partial t}|u(\theta,t)\rangle = \hat{H}\,|u(\theta,t)\rangle \tag{2.14}$$

where $|u(\theta,t)\rangle$ is the state of the system at t. By neglecting the kinetic energy operator immediately around the kick we obtain

$$i\,\hbar\,\frac{\partial}{\partial t}|u(\theta,t)\rangle = K\cos(\theta)\delta(t - nT)|u(\theta,t)\rangle. \tag{2.15}$$

If we now set $|u_n\rangle$ to be the state of the system immediately before the kick n and $|u_n^{'}\rangle$ to be the state immediately after kick n we get

$$|u_n^{'}\rangle = exp[\frac{-i\,K\,T\cos(\theta)}{\hbar}]\,|u_n\rangle. \tag{2.16}$$

Between kicks the system evolves freely, because there is no external force. This leads to

$$|u_{n+1}\rangle = exp[-i\,\hat{L}^2\,T/2\,I\,\hbar]|u_n^{'}\rangle \tag{2.17}$$

where $|u_{n+1}\rangle$ is the state of the rotor immediately before kick $n+1$. From equations (2.17) and (2.16) we construct the complete unitary time propagator over one kick

$$\hat{U} = exp[-i\,\hat{L}^2\,T/2\,I\,\hbar]\,exp[-i\,K\,T\cos(\theta)/\hbar]. \tag{2.18}$$

Now we introduce the dimensionless angular momentum operator

$$\hat{L} = \hbar\,\hat{l} \tag{2.19}$$

and the two dimensionless control parameters

$$\tau = \frac{\hbar T}{I}\ ,\ k = \frac{K\,T}{\hbar} \tag{2.20}$$

using these the time propagator (2.18) can be written as

$$\hat{U} = exp[-i\,\tau\,(\hat{n} + \beta)^2/2]\,exp[-i\,k\,\cos(\theta)]. \tag{2.21}$$

From the quantum mapping $\hat{U}$ we can obtain analogous to the classical map (2.6)

$$\begin{aligned} l_{n+1} &= l_n + k\,\sin(\theta_n) \\ \theta_{n+1} &= \theta_n + \tau\,l_{n+1} \end{aligned} \tag{2.22}$$

where l is not an operator but a complex number. To write this in the same form as the classical map we need to introduce $\tilde{l}_n = \tau\, l_n$. Substituting this into (2.22) to obtain

$$\begin{aligned} \tilde{l}_{n+1} &= \tilde{l}_n + S\, \sin(\theta_n) \\ \theta_{n+1} &= \theta_n + \tilde{l}_{n+1} \end{aligned} \tag{2.23}$$

where $S = k\,\tau$. As can be seen the mapping of the quantum kicked rotor has two dimensionless control parameters. They cannot be transformed into one by a scaling transformation, since τ is an independent parameter. In addition we also have one parameter which is not present in the classical case, the quasimomentum β.

2.2.2 Properties

Dynamical localisation

The change in energy as a function time, for most value of the parameters τ and β, is in general an initial linear growth followed by fluctuation around a constant value. It means, that independent of the kicking strength, the system eventually stops absorbing energy. The wave function is localised in momentum space, commonly referred to as "dynamical localisation". This an essentially property for the purpose of the project, since without this property the system cannot be opened (as explained in 2.2.3).

Quadratic energy growth

As explained above for most choice of the parameters τ and β the system exhibits dynamical localisation. For τ commensurate to $2\,\pi$ though, the system exhibits quadratic energy growth [5], which is referred to as "quantum resonance". This affect is also important in the further study of the system. To avoid distorting the results obtained in analysing the system, it is necessary to avoid values of τ commensurate to $2\,\pi$, when scanning through parameter space.

2.2.3 Survival probability

Opening System

The aim to study the system requires the study of the system under external perturbation. It has to be ensured though, that the external perturbation does not significantly change the properties of the system. For the kicked rotor due to the dynamical localisation, it is possible to have system which decays and the decaying process can be studied.

Survival probability

The decay process is implemented by neglecting components of the momentum, which lie outside of a certain interval $]n_1, n_2[$. This is achieved, by setting the wave function to zero for these components of the momentum. The wave function does not need to be normalised after this process, since the maximum for the Energy lies

at $\approx$ ñ and decreases exponentially to both sides. Therefore, asserting the interval $]n_1, n_2[$ is chosen large enough, the introduced perturbation is indeed small and negligible.
To measure the effects of the decay due to the boundaries we choose the "quantum survival probability"

$$P_{surv}(t; \tau, \beta, k, n_1, n_2) = \sum_n |\psi(n; t)|^2. \tag{2.24}$$

This represents the remaining momentum states inside the system after the decay process at time t.

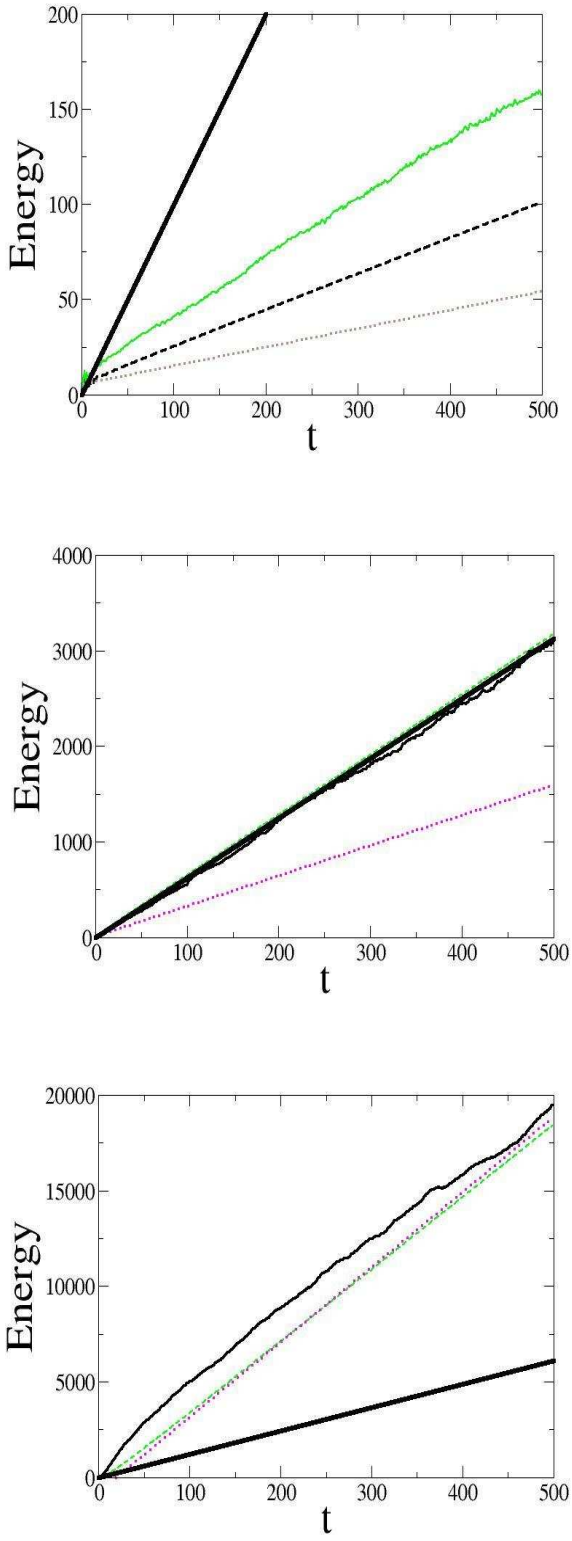

Figure 2.3: plot of Energy E against number of kicks n
left: $S = 2$, center: $S = 5$, right: $S = 7$

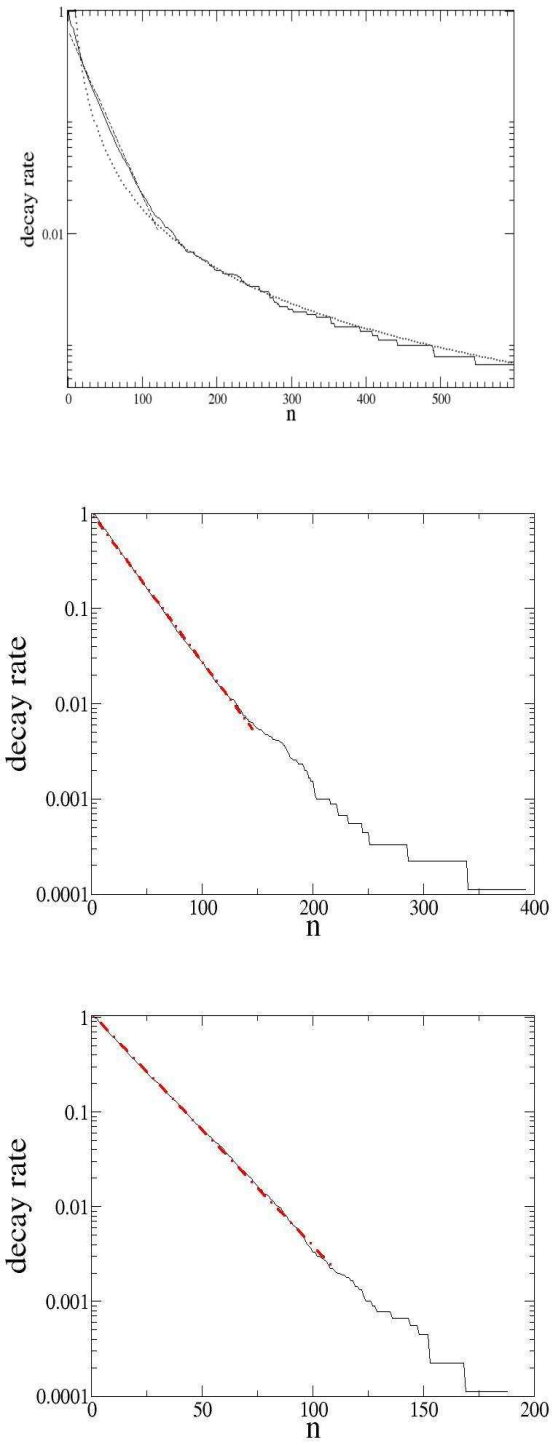

Figure 2.4: plots of decay rate (on a logarithmic scale) against n
left: $S = 2$, centre: $S = 4$, right: $S = 7$ solid line: decay rate, dashed line: exponential best fit, dotted line: best fit power law

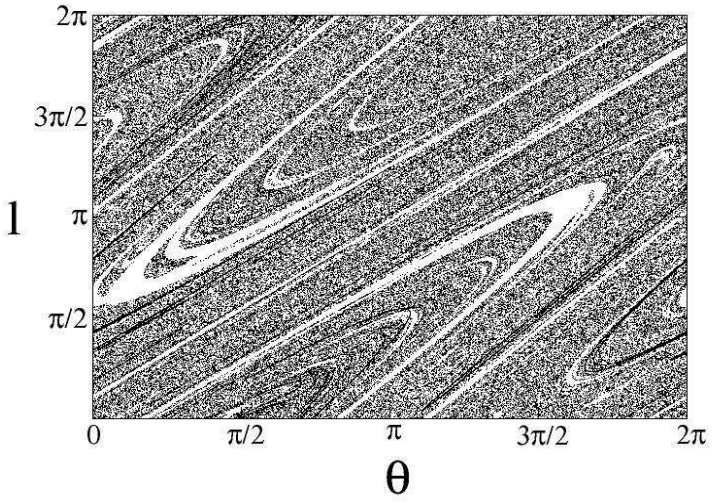

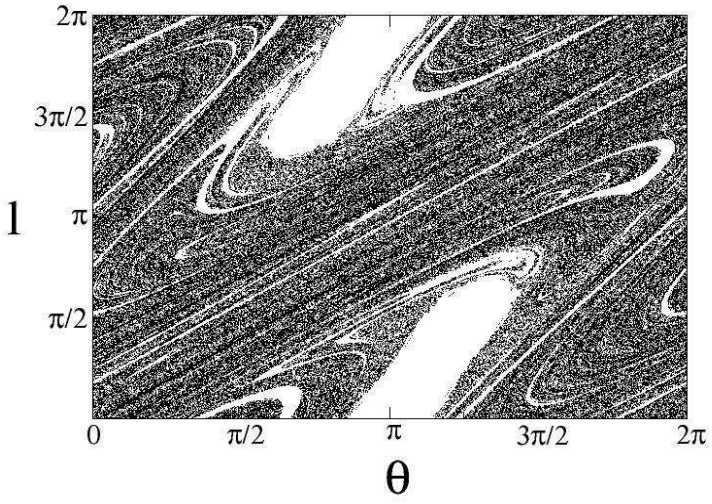

Figure 2.5: plot of phase space after decay
left: $S = 7$, right: $S = 4$

Chapter 3

Numerical method

3.1 Classical kicked rotor

The map of classical δ-kicked rotor shown in eqn (2.6) can be directly implemented into an algorithm, by incrementing the momentum and position in the loop. To enable having different initial conditions l_0 and θ_0, a loop over the initial values is implemented. To get a phase space plot the values of (l_n, θ_n) are outputted after each kick. Since in classical phase space the chaotic and regular parts in phase space are separated by an impenetrable seperatrix. To ensure a complete phase space picture, initial values have to be chose, that are both in the chaotic and regular part of phase space.

3.2 Quantum kicked rotor

3.2.1 Time evolution

The algorithm used to implement the time evolution of the Quantum kicked rotor is explained in the following. To start up, the periodic factor of the wave function is rewritten as

$$u(\theta) = \sum_{n=n_{min}}^{n_{max}} u_n \, e^{2\pi n x} \tag{3.1}$$

where u_n is a vector representing the expansion coefficient in the momentum space. The vector would need to be infinite for a complete description of the system, but for the purpose of this project, it is sufficient as long as $n_{min} \ll n_1$ and $n_{max} \gg n_2$ (for definition of n_1 and n_2 see sec. 2.2.3). For most results the basis is chosen such that n_{min}=-1024 and n_{max}=1023, so the interval spans a basis of 2048. For some cases the interval was doubled, which will be further discussed in the following chapter. In all the following discussion expansion coefficient is initially set to $u_n(t = 0) = \delta_{n0}$, which means that initially the wave function represents a particle at rest.
The implementation of the time evolution from eqn. (2.21) is done in two steps by looking at the two factors of $\hat{U}$. The first step is the free evolution in momentum space. For this we look at the momentum dependant factor of $\hat{U}$, which is diagonal in momentum space so it can be multiplied with the expansion coefficient in the

following way

$$\left(\hat{U}\,u\right)_n = exp\left[\frac{-i\,\tau\,(n+\beta)^2}{2}\right]\;u_n. \tag{3.2}$$

The second step is the instantaneous kick, for which it is necessary to transform the expansion coefficient into position space. This is implemented by using a Fast Fourier Transform as a subroutine, thus transforming expansion coefficient in momentum space u_n to the expansion coefficient in position space u_j. The θ dependant factor of $\hat{U}$ is diagonal in position space and can be multiplied with the expansion coefficient but this time in position space

$$\left(\hat{U}\,u\right)_j = exp\left[-i\,k\,\cos(\theta)\right]\;u_j \tag{3.3}$$

Now the Fast Fourier Transform is implemented again, which transforms the expansion coefficient back into momentum space. In momentum space the absorbing boundary conditions are applied, this is achieved, by setting u_n=0 $\forall\; n \leq n_1$ and $n \geq n_2$. The resulting expansion coefficients are used to calculate the average energy and the probability of states, which is than used to calculate the survival probability. The survival probability is calculated as a function of τ, to ensure that the underlying phase space remains the same, k has to be varied as well, to compensate for the change in τ. This comes from the fact that the parameter S determines the phase space of the classical δ-kicked rotor, and in the quantum mechanical case $S = k\,\tau$. The time evolution is implemented in C++ with an external subroutine for the Fast Fourier Transform in fortan70.

3.2.2 Analysing fractal dimension

The curves of the survival probability show, as mentioned before, fractal structures. To evaluate the Hausdorff dimension of a geometric set, the standard procedure is to use the box-counting algorithm. In this case with the graph of a real function, it becomes particularly simple. The interval of τ, $[\tau_{min}, \tau_{max}]$ is split into subintervals I_i of equal width δ. Computing

$$N(\delta) = \sum_i \frac{\lceil(\max\,P_{surv}(\tau_n) - \min\,P_{surv}(\tau_n))\rceil}{\delta}\;\tau_n\,\epsilon\,I_i \tag{3.4}$$

with varying δ leads to the power law $N(\delta) \sim \delta^{-D_f}$, only if the graph of $P_{surv}(\tau)$ shows a fractal structure. The plot of $\log[N(\delta)]$ against $\log[1/\delta]$ is straight line with slope D_f. Though for large δ the slope is 2 and for small δ it is 1 (see Fig (3.1)). The box counting algorithm is tested on a random walk with D_f=1.5, the fractal dimension is obtained correctly to the first decimal place. The box counting algorithm underestimates fractal dimensions for graphs with $D_f \geq 1.5$ [8]. Getting a more accurate estimate is difficult because of uncertainties when fitting.
The fractal dimension can also be calculated by two alternative ways using the correlation, C and variance, V. They are derived from the Brownian-motion like nature of the fluctuation curves, it can be shown in the semiclassical case [9].

$$\begin{aligned} C(\Delta\tau) &= \langle P_{surv}(\tau).P_{surv}(\tau+\Delta\tau)\rangle_\tau \\ V(\Delta\tau) &= \langle|P_{surv}(\tau+\Delta\tau) = P_{surv}(\tau)|^2\rangle_\tau \end{aligned} \tag{3.5}$$

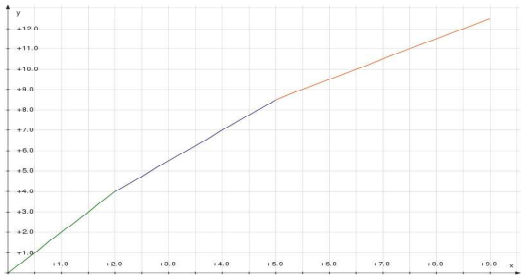

Figure 3.1: General structure expected for a plot of $\log[N(\delta)]$ against $\log[1/\delta]$

In the limit of $\Delta\tau \rightarrow 0$, both methods should yield a power law, with exponent α

$$1 - C(\Delta\tau)/C(0) \sim c\Delta\tau^{\alpha}, \;\; V(\Delta\tau) \sim c\Delta\tau^{\alpha} \tag{3.6}$$

where c is a constant. The fractal dimension can be calculated from α by

$$D_f = 2 - \alpha/2. \tag{3.7}$$

The double logarithmic plot of the relations eqn. (3.6) yields straight lines which tail off, for large $\Delta\tau$. The part of the graph which follows the straight do have a slope of α. The exponent for correlation is labeled α_{corr} and the exponent for variance is labeled α_{var}.

3.2.3 Floquet operator

The non-unitary Floquet operator is computed including the projection inside the absorbing boundary conditions. It is than diagonalised for several values of τ, generating the eigenphases $E_\tau - i\Gamma_\tau/2$, where E_τ represents the quasienergies and Γ_τ represents the decay widths. This is done to ensure that the system does yield fractal reaction curves. One condition is that the distribution of the density of decay widths, $\rho(\Gamma)$, follows the power law $\rho(\Gamma) \propto \Gamma^{-\alpha}$. Another condition is that the real parts of the energy spectrum are uncorrelated. To verify the first condition $\rho(\Gamma)$ is plotted against Γ on a double logarithmic plot. As expected this yields a straight line, with $\alpha \approx 1$ for both sets of parameters. To verify the second condition, firstly all the energies are sorted such that $E_{\tau,j} < E_{\tau,j+1}$. Then the probability densities renormalised quasi energy spacings $P(s_{\tau,j})$, where $s_{\tau,j} = \Delta E\tau, j/\langle\Delta E\rangle$ is plotted against s. Typically the probability densities of differences of uncorrelated variables should follow a Poisson distribution of the form $P(s) = e^{-s}$. Both plots are shown in fig. (3.2) for $S = 2.2$ and $S = 4$.

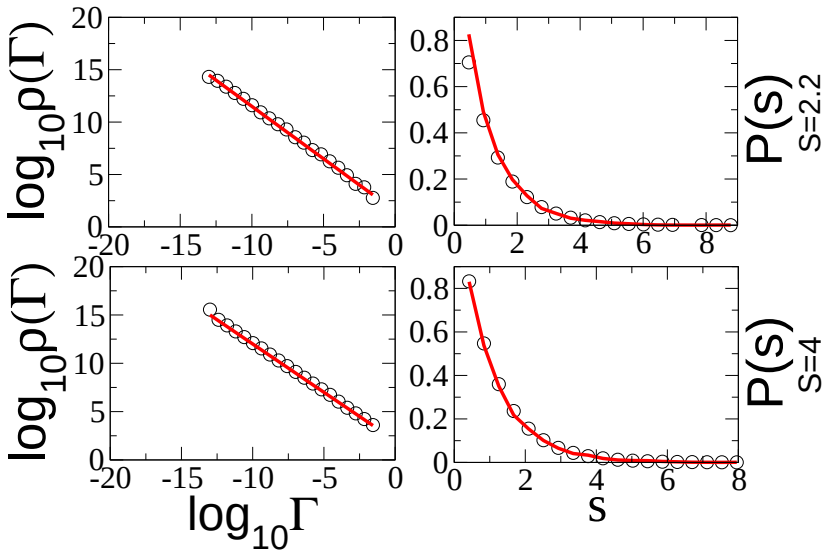

Figure 3.2: $\log[\rho(\Gamma)]$ against $\log[\Gamma]$ and $P(s)$ against s for two sets of parameters.

Chapter 4

Results

Answering the question about the behaviour of the complexity of the quantum kicked rotor for underlying mixed classical phase space is the subject of this project and will be the main focus in this chapter. The complexity of the quantum kicked rotor is studied by analysing survival probability curves as a function of τ, k and β (explained in detail in sec. 4.1). The fractal dimension of these curves is a measure for the complexity of the system. The results from the classical δ-kicked rotor are used to choose parameters to determine the phase space structure and initial condition. In essence this project is an extension of the work done in [10]. In previous studies the fractal fluctuations studied were for systems with an underlying phase space, which is completely chaotic. In this project the range of parameters is increased to include systems with and underlying mixed phase space and the problem approached more systematically.

4.1 Method

$P_{surv}(\tau, k)$ are calculated at fixed phase space and initial conditions. The resulting curves are analysed using the three methods mentioned in ch. 3.2.2, namely the box counting analysis, the temporal correlation and variance. In this section the methods used and some of the problems encountered are discussed in detail.
As mentioned in sec. 2.2.2, for τ comparable to 2π quantum resonances occur, therefore when survival probabilities are calculated these values of τ need to be avoided. The effect of including these values would change the structure of the $P_{surv}(\tau, k)$ significantly, since for these parameters the trajectories would decay very quickly even after small times. The grid for τ has to be chose in such a way, that these values are avoided. The golden ratio, $(\sqrt{5}-1)/2$ is the "most irrational" number because it shows the slowest convergence in the expansion of continued fractions of all irrational numbers. To ensure the resonant values of τ are avoided, the golden mean is used to calculate the separation between successive values of τ.

4.1.1 Boxcounting

The definition of the boxcounting includes a ceiling function when counting the number of boxes needed to cover the curve. When this is implemented numerically, the resulting curves of $\log[N(\delta)]$ against $\log[1/\delta]$ do not follow the predicted trend

of Fig. (3.1). This is only the case, when the spread of $P_{surv}(\tau, k)$ is similar to the step size in τ. For these curves the predicted $D_f \approx 2$ for large δ are not observed. This is only the case, when the ceiling function is used (see eqn. (3.4)), when leaving out the ceiling function, the predicted structure in the double logarithmic plot of $N(\delta)$ against $1/\delta$ is observed. To evaluate the slope to get D_f, these regions need to be avoided. This is done systematically by comparing curves with and without the ceiling function for different parameters to identify a value of $\log[1/\delta]$ which separates the region in which both curves follow the same trend from the region where they differ. This applied to two different sets of parameters can be seen in Fig (4.1.1). As mentioned in sec. 3.2.2, it is difficult to get the value of the fractal

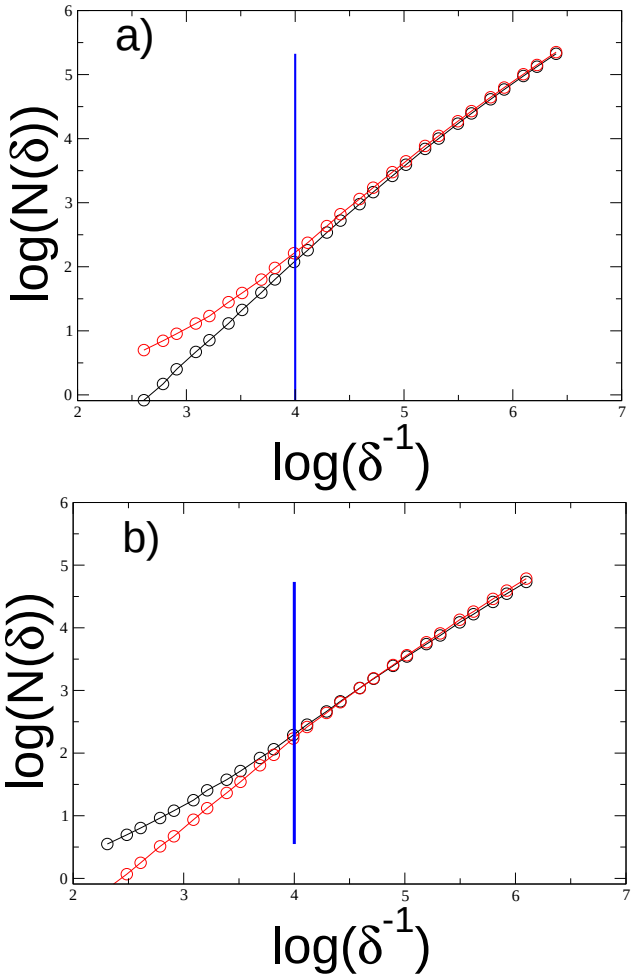

Figure 4.1: The comparison between the two different methods for box counting are show for two sets of parameters. Panel a) shows the plots for S=5, $\tau\epsilon\,[0.886, 0.896]$, after 10 000 kicks. Panel b) shows the plots for S=5, $\tau\epsilon\,[1.40, 1.42]$, after 5000 kicks.

dimension precise to more than the first decimal point.To identify the best fit for the slope, the cutoffs are varied changing the size of the interval for the fit. The

cutoffs are chose to ensure, that D_f is stable to a change in the size of the interval. A plot of D_f against interval size is show in Fig. (4.2).

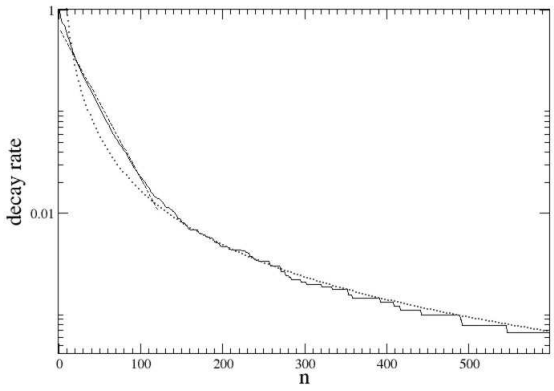

Figure 4.2: Wrong picture, needs to redone

4.1.2 Correlation

To compute the fractal dimension from the analysis of the correlation as mentioned in 3.2.2, is not possible for some of the survival probability curves. One example of

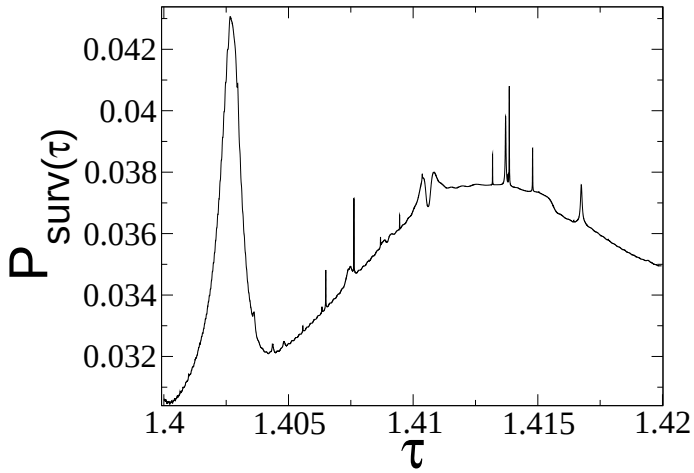

Figure 4.3: Survival probability as a function of τ for $S = 3$ after 3000 kicks

such a curve can be seen in fig. (4.3), where the large peak for small τ makes the analysis of the correlation impossible. As can be seen in fig. (4.4), the correlation has an initial positive slope, which is not as expected in a normal correlation. This

initial increase makes it impossible to study the double logarithmic plot of eqn. (3.6), because it would be initially negative. To make sure that the correlation of this function can be studied despite this problem, a shift in the survival probability is introduced. It is implemented by subtracting $\langle P_{surv}(\tau, k)\rangle_\tau$ from all the values of the survival probability. This centres the curve around x-axis, ensuring the appropriate structure of the correlation function as can be seen in fig. (4.4).

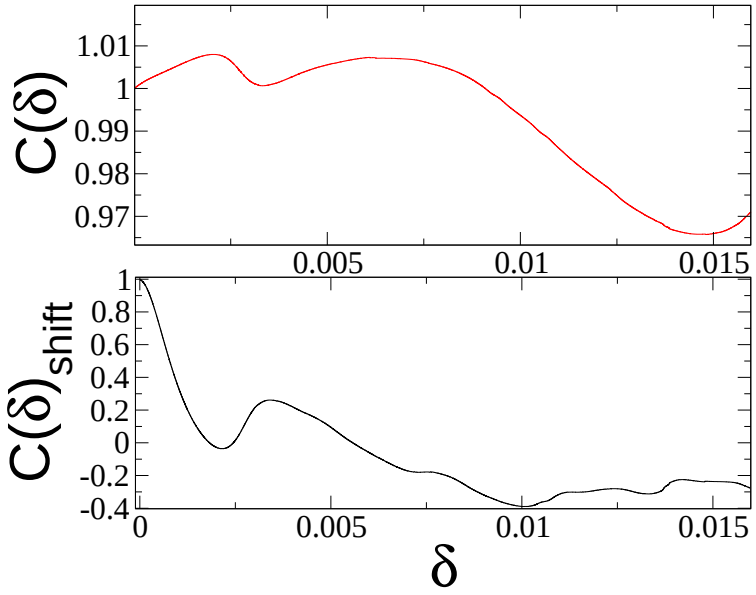

Figure 4.4: Correlation

4.1.3 Localisation

For the analysis of the survival probability curves, as mentioned in ch. 2.2.2, the localisation of the wave function inside the absorbing boundaries is a necessary condition. For large values of S the boundaries initially used $]-1, 200[$ do not ensure localisation over a sufficiently large range as can be seen in Figure (4.5). The first plot shows the probability for states logarithmically against the state, and it is visible, that the wave function is only localised for n between roughly 150 and 200. This localisation is not large enough. In the second plot, for small Γ the plot tends towards a constant value, though the expected trend is shown as a solid line. Both these effects can be avoided, by increasing the size of the interval $]n_1, n_2[$. Increasing n_2 only, does not have a large effect on the localisation of the wave function, because, most of the decay takes place at the boundary n_1. This can be seen in fig. (4.6), where the localisation is only extended to the right for larger n, but it has no effect on the wave function for small n. When changing n_1 care has to be taken not to make much small than -1, because otherwise the amount of decay would be minimal, and the resulting curves for the survival probability would be meaningless. This can be seen in table 4.1, where for n_1=-50 the survival probability is close to 1.

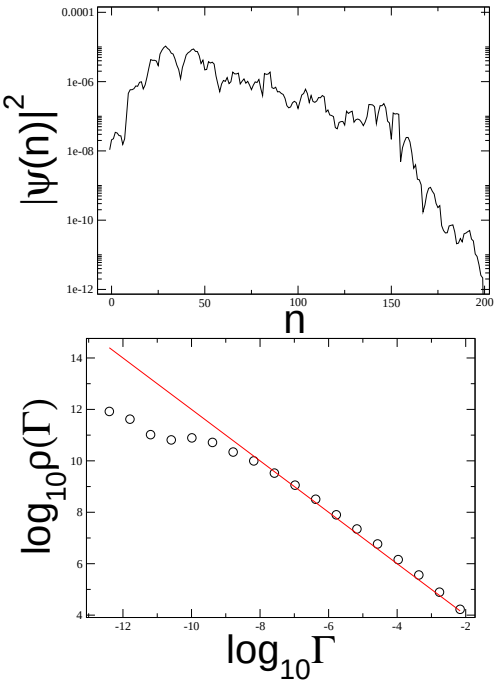

Figure 4.5: Wave function

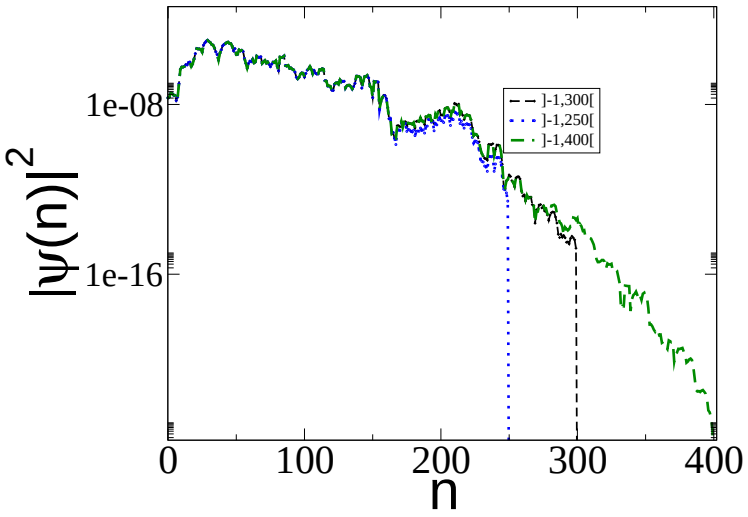

Figure 4.6: Wave function in momentum space for different values of the cut off

4.1.4 Quasimomentum

Initially the only parameters varied in the system are τ and k. This is done, to ensure that the underlying phase space is constant. For $S \leq 4$ this is no sufficient, because $p_0 = l_0/\tau = n + \beta$, where p_0 is the momentum of the quantum kicked rotor and l_0

S	τ	n_1	n_2	250 kicks	1000 kicks	5000 kicks	10 000 kicks
2.2	0.886	-1	200	0.2967292	0.1670350	0.0175889	0.0087693
5	0.886	-1	200	0.0090429	0.0029328	0.0005758	0.0003611
10	0.886	-1	200	0.0082947	0.0016362	0.0002481	0.0001136
2.2	1.400	-1	200	0.4867750	0.1203949	0.0326365	0.0265505
5	1.400	-1	200	0.0079890	0.0015688	0.0003452	0.0001507
10	1.400	-1	200	0.0094683	0.0016767	0.0003033	0.0001843
2.2	0.886	-10	500				
5	0.886	-10	500				
10	0.886	-10	500				
2.2	1.400	-10	500				
5	1.400	-10	500				
10	1.400	-10	500				
2.2	0.886	-25	500				
5	0.886	-25	500				
10	0.886	-25	500				
2.2	1.400	-25	500				
5	1.400	-25	500				
10	1.400	-25	500				
2.2	0.886	-50	500				
5	0.886	-50	500				
10	0.886	-50	500				
2.2	1.400	-50	500				
5	1.400	-50	500				
10	1.400	-50	500				

Table 4.1: Survival probability for different values of $]n_1, n_2[$

the momentum of the classical δ-kicked rotor. For $p_0 \neq 0$, β should be non-zero as well, because otherwise for changing tau, the equation would not hold. β has to be set, to represent the decimal part of p_0. For all parameters with $S \leq 4$, the survival probability curves are plotted again, with changing β. The change introduced by this change in β varies according to the value of the parameters. In fig. (4.7), two plots are shown with two different sets of parameters, with different effects of changing the β. Changing the qusimomentum ensures, that the underlying phase space as well as the initial conditions remain constant.

4.2 Central results

The results were obtained for two different intervals of τ, firstly $\tau\epsilon[1.4, 1.42]$ and secondly $\tau\epsilon[0.886, 0.896]$. In both cases S is varied between 2 and 10 and number of kicks are varied between 100 and 10000. The plots of the survival probability show stronger fluctuations for higher S and for larger number of kicks. In general overlapping peaks start to appear for S =5, in both intervals of τ. A plot with hardly any fluctuations can be seen in fig. (4.3), an example on the other extreme with a large number of overlapping peaks can be seen in fig. (4.8). The trend for these preliminary results is an initial increase followed by a saturation. The point at

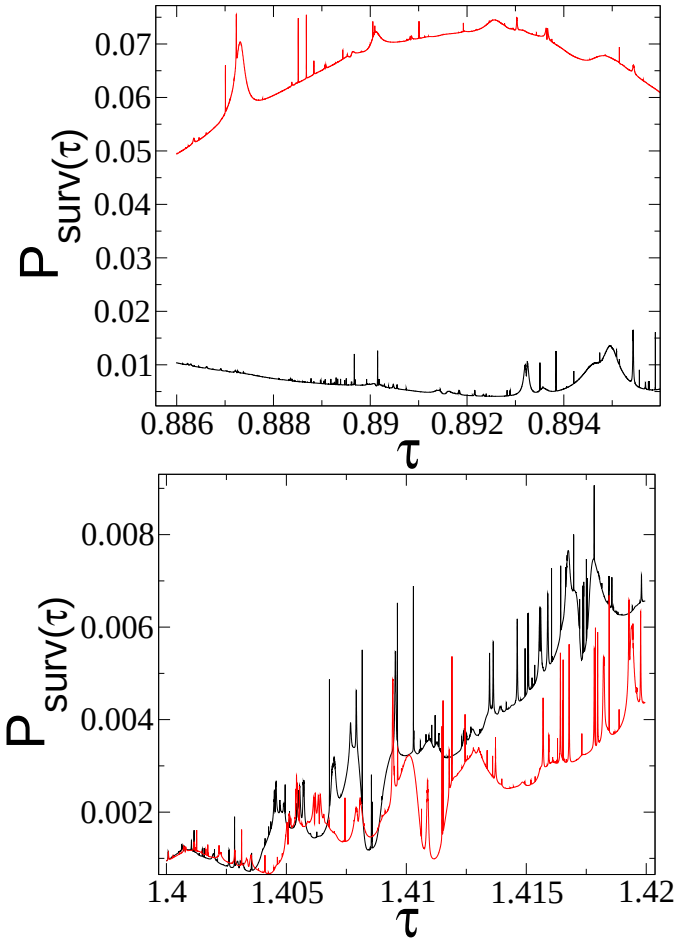

Figure 4.7: Two curves of $P_{surv}(\tau, k, \beta)$ against τ. Top curve for $\tau\epsilon\,[0.886.0.896]\,, S = 3$ after 10000 kicks. Bottom curve for $\tau\epsilon\,[1.40.1.42]\,, S = 4$ after 6000 kicks

which the saturation starts differs between the two intervals. The error is estimated by comparing two most extreme fits and taking the difference to be the error. The resulting error is quite large, but this only shows the difficulty of finding a fit. The results of the fractal analysis using correlation and with the same parameters is shown in fig. (4.10). For correlation of the interval $\tau\epsilon[0.886, 0, 896]$, the first value is problematic as can be seen in table (**??**), for small S and small number of kicks, the correlation does not measure the fractal dimension well. The same problem occurs for some values of the correlation with shift (see table (**??**)). Doing the analysis with varying β does not introduce a big difference in the trend of the data as can be seen in fig. (4.11). The new data points connected here by a solid red line, lie almost without exception well within the errors of the original points.

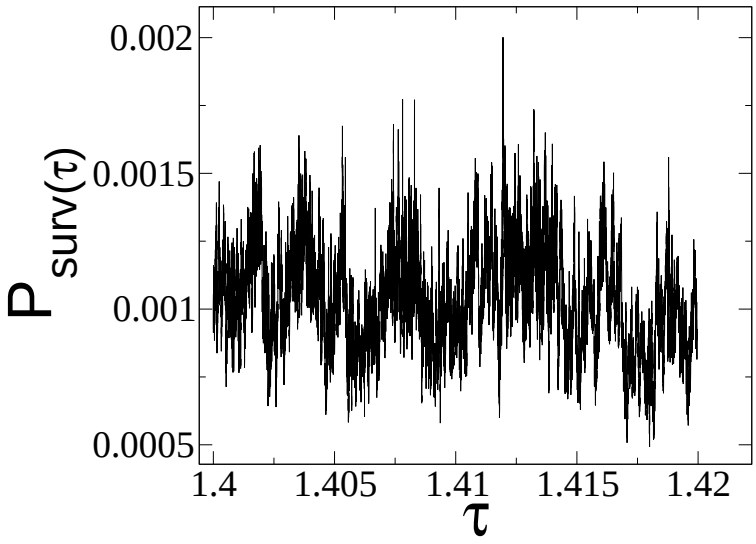

Figure 4.8: $P_{surv}(\tau, k)$ against τ for S=9 after 3000 kicks

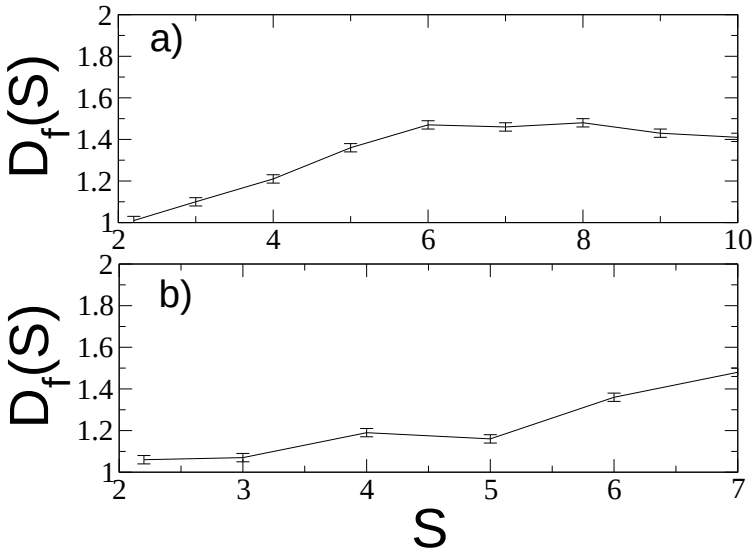

Figure 4.9: $D_f(S)$ for increasing S. Panel a) for $\tau\epsilon[0.886, 0.896]$. Panel b) $\tau\epsilon[1.4, 1.42]$

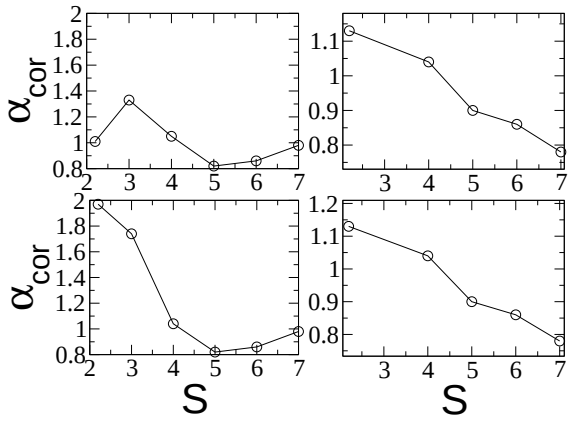

Figure 4.10: correlation and variance for both intervals

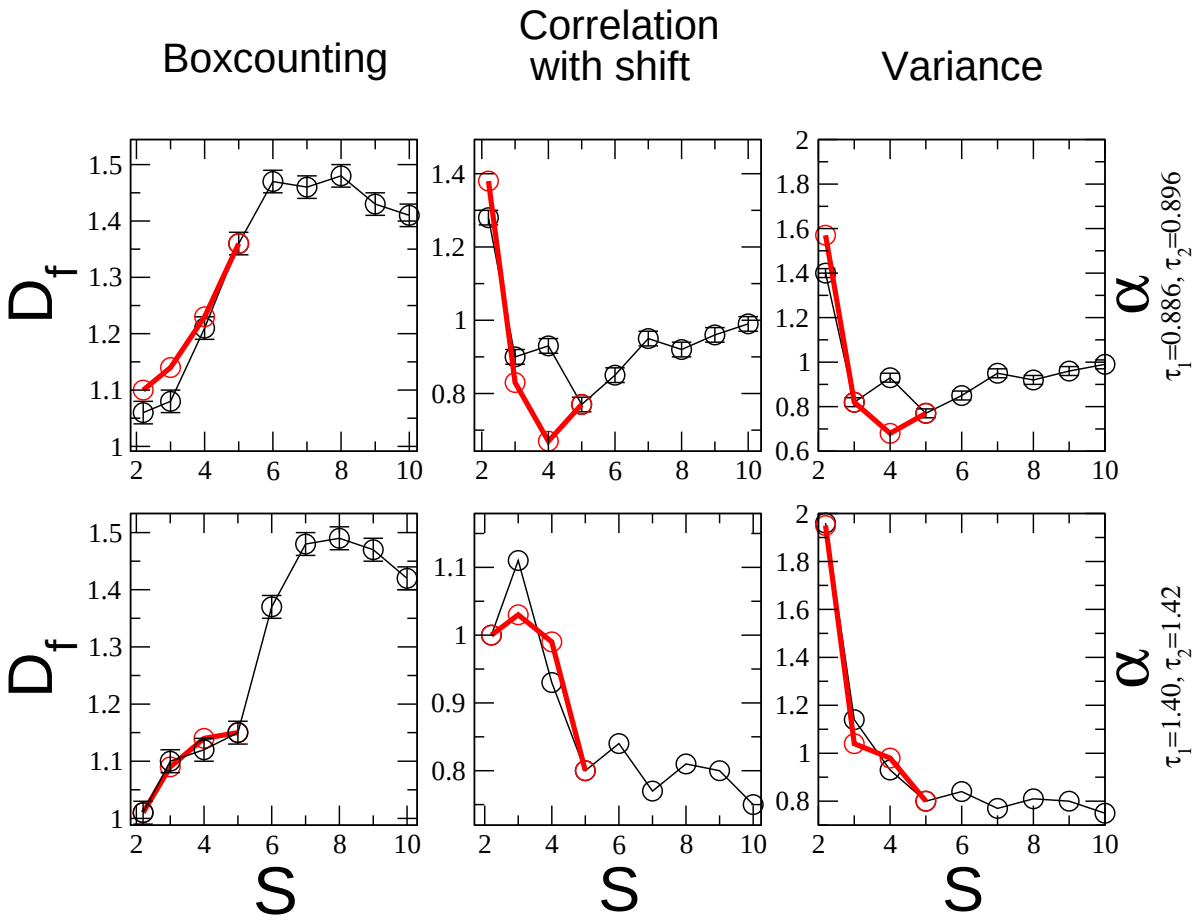

Figure 4.11: Analysis of fractal dimension with all three methods. Bold red line connects data points for varied β.

Chapter 5

Conclusion

Bibliography

[1] Edward Ott. *Chaos in Dynamical Systems*. Cambridge University Press, Cambridge, Second Edition 2002.

[2] Reinhold Blümel, William P. Reinhardt. *Chaos in atomic Physics*. Cambridge University Press, Cambridge, 1997.

[3] Gabriel G. Carlo, Giuliano Benenti, Giulio Casati, Sandro Wimberger, Oliver Morsch, Riccardo Mannella, Ennio Arimondo. Chaotic ratchet dynamics with cold atoms in a pair of pulsed optical lattices. *Phys. Rev. A* 74, 033617, 2006.

[4] B.V. Chirikov. A universal instability of many-dimensional oscillator systems. *Phys. Rep.* **52**, 263- 379, 1979.

[5] S. Fishman, *Quantum Chaos: Proceedings of the International School of Physics 'E Fermi' CXIX* edited G. Casati, I. Guarneri, U. Smilansky *et al* (Amsterdam: IOS), (1992)

[6] B.V. Chirikov, D.L. Shepelyansky. Correlation properties of dynamical chaos in Hamiltonian systems. *Physica D13*, 195-400, 1984.

[7] A.B. Rechester, R.B. White. Calculation of turbulent diffusion for the Chirikov-Taylor model. *Phys. Rev. Lett.* 44, 1586-1589, 1980.

[8] B. Dubuc, J.F. Quiniou, C. Roques-Carmes, C. Tricot, S.W. Zucker. Evaluating the fractal dimension of profiles. *Phys. Rev. A* 39(3):1500, 1989.

[9] Y.C. Lai, R. Bümel, E. Ott, C. Grebogi. Quantum Manifestation of Chaotic Scattering. *Phys. Rev. B,* 31:006852, 1985

[10] A. Tomadin, R. Mannella, S. Wimberger. Can quantum fractal fluctuations be observed in an atom-optics kicked rotor experiment? *J. Phys. A: Math. Gen.* 39 2477-2491 (2006)